PAPER

Check for updates

New technology for preparing energetic materials by nanofiltration membrane (NF): rapid and efficient preparation of high-purity ammonium dinitramide (ADN)†

Hai-Yang Zhu,[ab] Ying-Hui Liu,[ab] Hai-Yun Sun,[ac] Dan-Dan Cao,[b] Yu-Chuan Li [ID] *[ab] and Si-Ping Pang [ID] *[a]

The development of environment-friendly and non-toxic green energetic materials and their safe, environmentally friendly, and economical production is very important to the national economy and national security. As an innovative, efficient, and environmentally friendly energetic material, the preferred preparation method of ammonium dinitramide (ADN) is the nitro-sulfur mixed acid method, which has the advantages of high yield, simple method, and easy access to raw materials. However, the large number of inorganic salt ions introduced by this method limits the large-scale production of ADN. Nanofiltration (NF) has been widely used in various industrial processes as a separation method with high separation efficiency and simple operation. In this study, NF was used for the desalination and purification of ADN synthesized by the mixed acid method. The effects of NF types, operation process (pressure, temperature, and feed solution concentration) on desalination efficiency, and membrane flux during purification were examined. The results showed that 600D NF could achieve the efficient desalination and purification of ADN. It was verified that the highest desalination and purification efficiency was achieved at 2 MPa pressure, 25 °C, and 1 time dilution of the feed solution, and the membrane flux of the desalination and purification process was stable. Under the optimized process conditions, the removal rate of inorganic salts and other impurities reached 99% (which can be recycled), the purity of ADN reached 99.8%, and the recovery rate reached 99%. This process has the potential for the large-scale production of ADN and provides a new process for the safe, efficient, and cheap preparation of energetic materials.

1. Introduction

Energetic materials are special materials that contain explosive groups or oxidants and combustibles and can conduct chemical reactions independently and rapidly and output huge energy. In recent years, much attention has been paid to the development of new green energetic materials that are not only high energy, but also environmentally friendly and non-toxic, including explosives, propellants, and pyrotechnics, which are widely used in military and civilian explosive fields.[1,2] At the same time, the production technologies of energetic materials, such as

[a] School of Materials Science and Engineering, Beijing Institute of Technology, Beijing 100081, P. R. China. E-mail: liyuchuan@bit.edu.cn; pangsp@bit.edu.cn

[b] Lunan Research Institute, Beijing Institute of Technology, Tengzhou 277599, P. R. China

[c] Beijing Key Laboratory of Research and Application for Aerospace Green Propellants, Beijing Institute of Aerospace Testing Technology, Beijing 100074, P. R. China

† Electronic supplementary information (ESI) available. See DOI: https://doi.org/10.1039/d3ra01922e

safety, environmental friendliness and economy, have also received increasing attention.[3]

At present, there are hundreds of energetic materials that have been applied, such as the familiar ammonium nitrate (NH_4NO_3, AN), hexogen (RDX), octogen (HMX), and hexanitrohexaazaisowurtzitane (HNIW), with excellent energy. They can be used as both single compound explosives and high-energy oxidant components of composite explosives or propellants. New technologies, methods, and equipment for the synthesis and preparation of such materials are also emerging endlessly. Various synthesis methods for new energetic materials, such as the synthesis of new azotriazole energetic materials, fused ring energetic materials, energetic MOFs, and energetic salts have been reported.[4–8] New synthesis methods and preparation processes of high energy density materials (HEDM), such as the preparation of HMX using N_2O_5–HNO_3 system to nitrate urotropine at high yield, the two-step synthesis of HNIW to reduce production costs, and the large-scale preparation technology of high-quality HMX, have been explored.[9–12] In the process of producing HEDM, various technologies, such

as energy conservation and emission reduction, continuous production technology, recycling, pollution control, and treatment technology, and the use of new devices and equipment, have been adopted,[13–20] and good results have been achieved.

Taking propellant as an example, it is a polymer-based composite energetic material that can provide power for rocket and missile thrust.[21–23] High energy oxidizer is an integral part of propellant, and its structure and performance play a crucial role in the performance of the propellant. Redox reactions occur during the combustion of propellant, and the oxidizer provides an energy supply for the propellant.[24,25] The widely used oxidants must have high oxygen content, low heat of generation, high density, high gas production, *etc.* The commonly used oxidants are ammonium perchlorate (AP), AN, potassium perchlorate (KP), and RDX.[26–29] With continuous research on oxidants, green, high energy density, and safe and stable oxidants have been explored, and ADN appeared in the public eye as a new type of high-energy oxidant.[30,31] ADN appears as a new type of high-energy oxidant in the field of energy-containing materials, representing the international advanced level of oxidants, with the advantages of high oxygen balance value, high energy density, no halogen elements, clean gas, friendly to the environment, high density, *etc.* It is both a high-energy oxidant and a slamming explosive and has good prospects for application in propellants, high-energy explosives, and weapon charges in water.[32–34]

The synthesis methods of ADN include organic synthesis and inorganic synthesis, among which organic synthesis methods have not been developed on a large scale due to the drawbacks of low synthesis efficiency, complex synthesis routes, synthetic raw materials not being easily available, and not easy to be produced on a large scale.[35–37] The current means of ADN synthesis relies on inorganic methods, and the most common means is the separation and purification of crude ADN by using amino sulfonate as a raw material and nitrous sulfur mixed acid as a nitrifying agent under low temperature conditions, using ammonia to neutralize the product.[38–41] Amino sulfonates serve as key intermediates for the rapid formation of nitro functional groups. The $-SO_3$ group of amino sulfonates has strong electron absorption and can introduce two nitrate ions through a single reaction. Among the many reported synthetic routes for ADN, the synthesis of ADN using amino sulfonate as the initial raw material is still one of the more studied, safe and efficient methods, and is considered to be one of the most suitable methods for large-scale production, but it is easy to introduce a large number of excess ions in the nitration step, resulting in the final synthesis of ADN containing a large number of inorganic salts (mainly including AN, ammonium sulfate $((NH_4)_2SO_4, AS)$), which seriously affects the effectiveness of the use of ADN and becomes a key difficulty limiting the large-scale application of ADN.[42,43]

The special military characteristics of ADN led to a partial technology embargo, prompting fewer published studies on the purification of ADN. Some scholars have used MIBK precipitation and activated carbon adsorption methods for the desalination and purification of ADN, and have achieved significant treatment results and obtained ADN products with high

purity.[44–47] Although the above methods have the advantages of good purification effect, low processing cost, economic and environmental protection, and easy industrial scale-up production, they usually require more than two processing steps to complete the whole purification process, and the purification process cannot be carried out in continuous mode, and the extra step of adding chemicals or adsorbents in the process limits the promotion of the above technologies. In addition, the safety of the above processes and the treatment of waste acid and wastewater also need to be improved.

In the field of separation and purification at the molecular level, organic polymer-based nanofiltration (NF) separation technology has become one of the most commonly used techniques for the separation of inorganic salts in the solution due to its high separation efficiency, low construction, and operation costs, and ease of operation.[48,49] Currently, the mainstream view is that the core mechanism of salt ion separation by NF technology is size sieving, dielectric repulsion, electrostatic interaction, and the synergistic effect of all three. The separation of different ions in solutes is achieved by using the difference in the solute size in the solution and the membrane pore size, the difference in the dielectric constant of solutes in the solution and the dielectric constant of the membrane separation layer, and the difference in ionic charge of solutes in the solution and the fixed charge on the separation membrane.[50–53] The main ion types in the crude solution of ADN synthesized by the nitro-sulfur mixed acid method are dinitramides ($N(NO_2)^-$, DN^-), NH_4^+, NO_3^-, and SO_4^{2-}, which have different volumes, electrical properties, charge numbers, and charge densities in the solution state, making the desalting and purification of ADN by NF separation technology a theoretical possibility. In this study, the NF separation technology was used for the purification and desalination of ADN, the effect of NF separation technology on the desalination and purification of ADN was investigated, the operating parameters of NF separation technology for the purification of ADN were optimized, and the mechanism of NF separation technology for the purification of ADN was analyzed, which broadened the idea of efficient and simple continuous preparation of high-purity ADN and other HEDMs.

2. Experimental

2.1 Experimental setup

TYLG-19 flat NF separation tester (including NF tank, gear pump, and pressure gauge) was designed by our team and manufactured by Shandong Bona Biotechnology Group. The low-temperature thermostat tank (JULABO F81-HL) was purchased from JULABO Technology (Beijing) Co. Ltd. A polysulfone (PSF) ultrafiltration-based membrane was provided by Shandong Bona Biotechnology Group Co., Ltd (China).

2.2 Reagents and sources

ADN standards (≥99%) were prepared in our laboratory. Ammonium sulfamate ($NH_4SO_3NH_2$, ≥98%), nitric acid (HNO_3, ≥99%), sulphuric acid (H_2SO_4, ≥99%), *n*-hexane, sodium dodecyl
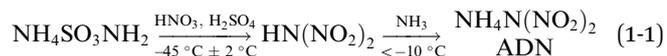
sulfate (SDS), triethylamine, Na_2CO_3, $NaHSO_3$, were purchased from Sinopharm Group Chemical Reagent Co. Anhydrous piperazine (PIP, ≥98%), *m*-phenylenediamine (MPD, ≥98%), and homo phthaloyl chloride (TMC, ≥99%) were purchased from J&K Scientific Ltd. Acetone and ammonia were purchased from Aladdin Reagent (Shanghai) Co., Ltd. The above reagents were of analytical grade and used without special instructions.

2.3 Experimental methods

2.3.1 ADN synthesis methods. First, 500 mL of concentrated nitric acid (HNO_3, 65–68% mass fraction) was added to a 5000 mL three-neck flask and cooled to a temperature no higher than 5 °C in a low-temperature cooling circulation bath (JULABO F81-HL). 175.0 mL of concentrated sulfuric acid (H_2SO_4, mass fraction about 98%) was carefully added dropwise to the nitric acid, taking care to control the temperature not rising higher than 10 °C during the drop addition. The mixed acid was stirred well and the temperature was controlled to −45 °C. Under vigorous stirring conditions, 100.0 g of ammonium sulfamate ($NH_4SO_3NH_2$, 175 mM) was added in batches, and the dosing process was controlled at 45 ± 2 °C. At the end of the dosing, the reaction was continued with stirring for 50 min. The pH was then adjusted to 6 with ammonia cooled to −40 °C, controlling the temperature at −10 °C during the process. The reaction mixture was purified by membrane separation to produce 64.0 g ADN with 59.0% yield and 99.7% purity.

The reaction equation is shown in eqn (1-1).

$$NH_4SO_3NH_2 \xrightarrow[-45\,°C \pm 2\,°C]{HNO_3,\ H_2SO_4} HN(NO_2)_2 \xrightarrow[<-10\,°C]{NH_3} \begin{array}{c} NH_4N(NO_2)_2 \\ ADN \end{array} \quad (1\text{-}1)$$

2.3.2 Detection methods. The determination of the anion content in ADN was performed by ion chromatography. The ion chromatograph model CIC-D160 was equipped with an SH-AP-1 column with the following detection conditions: 15–85 mM KOH solution as eluent, injection volume of 25 μL, column temperature of 35 °C, a flow rate of 0.7 mL min^{-1}, and a conductivity detector with a suppression current of 135 mA.[54] The standard solution ion chromatograms of DN^-, NO_2^-, NO_3^-, and SO_4^{2-} were plotted in Fig. S1.† The standard curves of DN^-, NO_2^-, NO_3^- and SO_4^{2-} were plotted in Fig. S2.†

2.3.3 Preparation of composite NF. The composite NF was prepared by the interfacial polymerization method. First, the ultrafiltration membrane was immersed in pure water for more than 12 h to remove the pore-preserving agent and residual solvent inside the membrane and then dried. Then, the base film was submerged in the mixed aqueous solution of PIP, MPD, SDS, and triethylamine for a certain period of time, and a soft rubber roller was rolled on the surface of the submerged film to eliminate the small bubbles formed during the soaking process, and the excess droplets on the surface of the base film were removed with filter paper and left for a certain period of time at room temperature. Next, the base membrane was immersed in TMC, Na_2CO_3 mixed with *n*-hexane solution for a certain time for the polymerization reaction. Subsequently, the membrane was removed and cured at a certain temperature for a certain time to obtain the nascent NF. Finally, the synthesized composite NFs were thoroughly washed with deionized water and stored in an aqueous solution containing 1 wt% $Na_2S_2O_5$. The preparation flow chart of NF is illustrated in Fig. 1.

Four types of NFs were prepared by the above method, namely M1, M2, M3, and M4. Due to the appearance of wrinkles on the surface of the M4 NF membrane during the curing process, it was discarded.

2.3.4 Filtering methods. The water flux and solute retention performance of the obtained NFs were evaluated by standard permeation tests using a cross-flow filtration device with three parallel recirculating filtration units with an effective membrane area of 28.27 cm^2 at a constant temperature of 25 °C, a transmembrane pressure of 0.5 MPa, and a pH of 7.0 ± 0.2. Permeate tests were performed under a recirculation model where the retention fluid was circulated back to the tank through a pressure regulator and the permeate from each cell was collected for volume measurements and solute content
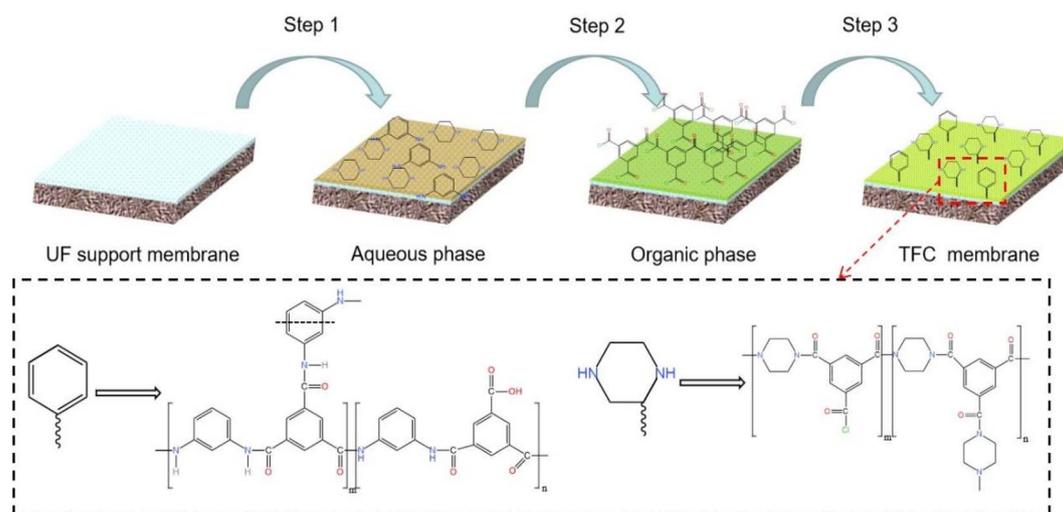

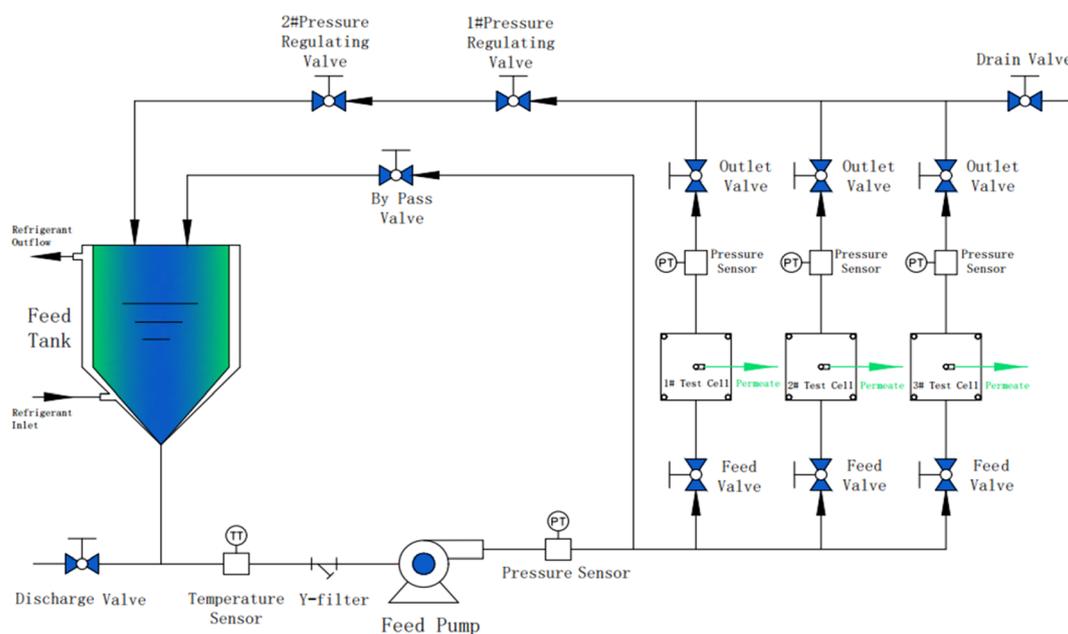**Fig. 1** The flow chart for the preparation of NF.

Fig. 2 The TYLG-19 flat plate NF separation tester and the flow chart of the separation tester.

measurements if necessary. The feed tank was returned to keep the feed concentration constant before the permeation test, and the circular diaphragm loaded in the filter cell was first pressurized with deionized water at a pressure of 1.0 MPa for 2 h to ensure a stable membrane flux. After that, the pure water flux was evaluated with deionized water.

The flow diagram of the experimental setup is illustrated in Fig. 2. NFs were installed into the NF cell, the fixing bolts were tightened, 500 mL of the solution to be filtered was added to the feed cell of the NF separator, the regulator was opened, the circulation pump was turned on, the solution was circulated to a stable state, the pressure was adjusted to the experimental setting, the permeate 400 mL and the concentrate 100 mL were collected and stored under refrigeration at 4 °C for testing or further filtration. The above experiments were repeated three times without special instructions to eliminate the experimental errors caused by uncertainty. In this study, all the original solutions of the NF experiments were filtered through a 0.45 μm microfiltration membrane before entering the feed cell of the NF separation experimental machine.

2.3.5 Solute retention rate and membrane flux. The solute retention rate (R) was calculated by eqn (1-2).

$$R = 1 - \frac{C_{\mathrm{p}i}}{C_{\mathrm{m}i}} \times 100\% \tag{1-2}$$

where $C_{\mathrm{p}i}$ is the concentration of substance i in the permeate and $C_{\mathrm{m}i}$ is the concentration of substance i in the feedstock.

The membrane flux (J) is calculated by eqn (1-3).

$$J = \frac{V}{At} \tag{1-3}$$

where V is the volume of permeate, A is the membrane area for effective filtration, and t is the filtration time.

3. Results and discussion

3.1 Characterization and performance tests of the NFs

M0, NF 200 (DuPont commercial membrane), M1, M2, and M3 are the test data of PSF basement membrane, 200D, 400D, 600D and 800D NFs, respectively.
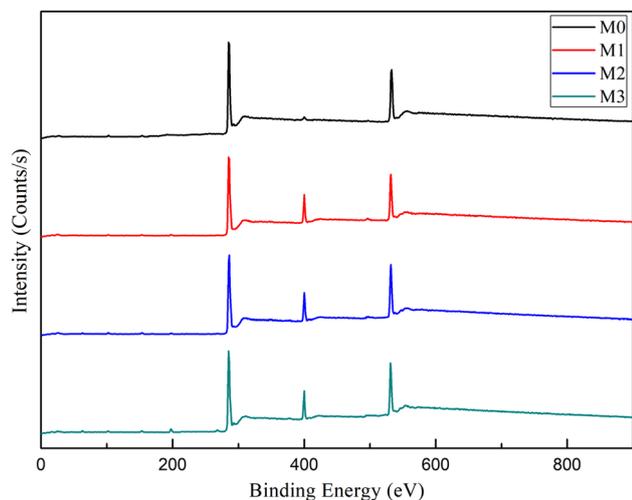

Fig. 3 The XPS patterns of the composite NF.

The membrane surface functional groups were characterized by X-ray photoelectron spectroscopy and the results are shown in Fig. 3. In the XPS spectra, the peaks of C 1s, N 1s, and O 1s in M0, M1, M2, and M3 membranes appeared at 285.0 eV, 400.0 eV, and 532.0 eV, respectively. There were very small N 1s peaks in M0 membranes, which may be caused by additives or solvent residues. There were significant N 1s peaks in M1, M2, and M3 films, indicating the synthesis of polyamide layers on the surface of the substrate. Proving the successful preparation of composite NF membranes.

The morphological structure of the composite membrane was studied using scanning electron microscopy (SEM) and the results are shown in Fig. 4. As shown in Fig. 4, with the extension of heat treatment time, the thickness of the ultra-thin polyamide functional layer of the composite NF membrane increases from about 80 nm to about 160 nm. The main reason for this change is that as the heat crosslinking time increases, the degree of crosslinking of the polyamide layer of the composite NF membrane increases. The increase in crosslinking degree and the membrane thickness of the polyamide layer is beneficial for improving the inorganic salt retention efficiency of the NF membrane, but it also increases the cross-membrane resistance of water molecules, resulting in a decrease in membrane flux. The specific degree of influence
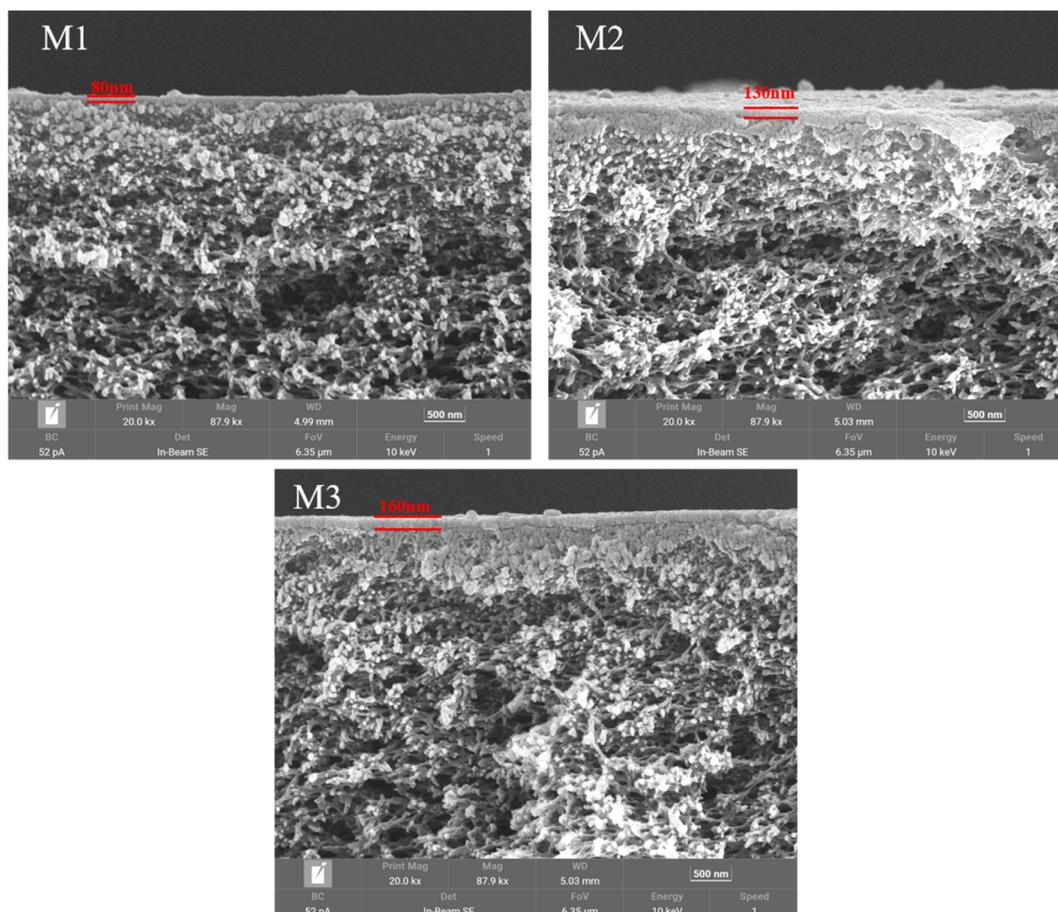

Fig. 4 A cross-sectional SEM image of the composite NF.
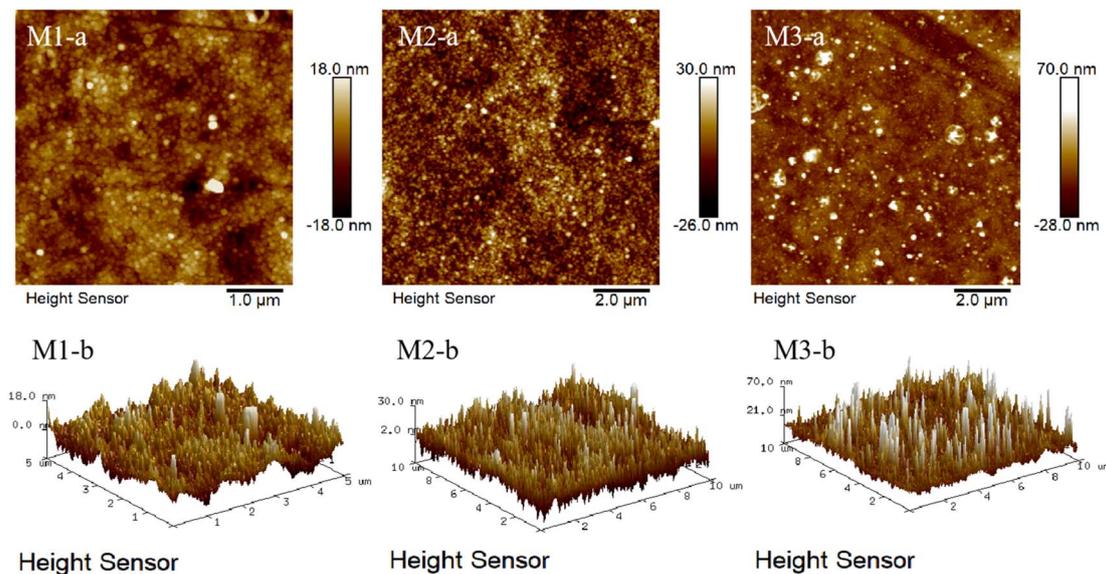
Fig. 5 The surficial AFM of the composite NF.

was studied and analyzed in the permeability of the composite NF membrane.

The surface morphology of the air-dried composite membrane was measured by atomic force microscopy (AFM) and the results are shown in Fig. 5. As shown in Fig. 5, with the extension of thermal crosslinking time, the number of granular protrusions on the surface of the membrane increases, indicating that the crosslinking degree of the composite NF membrane increases and the effective area of the membrane increases, and thus its roughness increases.

The dynamic contact angle measuring instrument was used to measure the water contact angle on the membrane surface at room temperature and the results are shown in Fig. 6. As shown in Fig. 6, with the extension of thermal crosslinking time, its hydrophilicity slightly decreases. This is mainly due to the increase in the roughness and film thickness of the generated polyamide separation layer, as well as the reduction of acyl chloride groups in the unreacted TMC, amino groups in PIP and
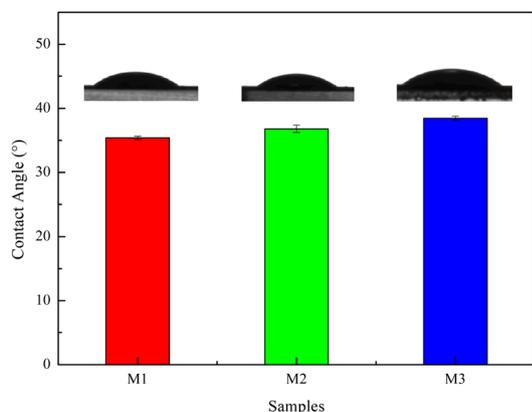
MPD on the surface, resulting in a slight decrease in hydrophilicity; at the same time, more amide bonds were generated on the surface, resulting in a slight decrease in the hydrophilicity of the membrane.

Surface flow potential measurements were performed using an electrodynamic analyzer to evaluate the surface zeta potential of the composite membrane and the results are shown in Fig. 7. The zeta potential is negative, indicating that the membrane surface charge is electronegative. The smaller the value, the stronger the electronegativity, and the more conducive to the interception of anions from water. It can be seen from Fig. 7 that the isoelectric points of the three composite NF membranes are almost at about pH = 4. When the pH is greater than 4, the surfaces of the three composite NF membranes are electronegative, which proves that the polyamide-selective layer was charged. Under neutral solution conditions, the surface charges of the three composite NF membranes were
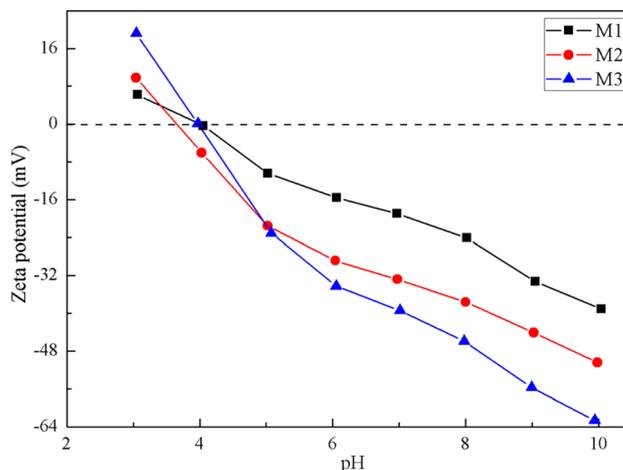

Fig. 6 Contact angle of the composite NF.

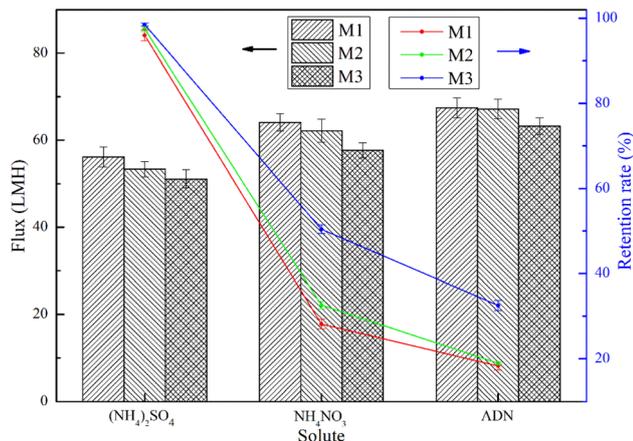**Fig. 7** Zeta potential of the composite NF.

Fig. 8 The permeability of the composite NF membrane to the salt solution.

significantly different. With the extension of the thermal crosslinking time, the zeta potential increased from −18.95 mV to −39.43 mV, indicating that the longer the thermal cross-linking time, the higher the crosslinking degree of the poly-amide layer and the stronger the electronegativity of the membrane surface. It showed that the increase in the thickness and density of the polyamide layer is conducive to the enhancement of the electronegativity of the membrane.

The permeability of the composite NF membrane to the salt solution is shown in Fig. 8. As shown in Fig. 8, it can be seen that the interception order of the three composite NF membranes for various salt solutions is $(NH_4)_2SO_4$ > NH_4NO_3 > ADN and the corresponding order of permeability flux for the salt solutions is ADN > NH_4NO_3 > $(NH_4)_2SO_4$. This is because, as the thermal crosslinking time prolongs, the crosslinking degree of the composite NF membrane increases, the separation layer thickens, the retention rate of the same salt increases, and the flux decreases. NF membranes have different retention properties for different salts, so they can be used to separate different salt solutions.

3.2 Effect of the NF aperture on the purification effect

In this study, the NFs of 200D, 400D, 600D, and 800D were used for filtration experiments on the raw synthetic solution without additional treatment to investigate the effect of pigment removal during filtration, and the results are shown in Fig. 9. As shown in

Fig. 9, the color of the concentrated solution is darker than that of the ADN mixed acid reaction solution, and the permeate is slightly greenish, indicating that the NF membrane has a good decolorization effect on the ADN mixed acid reaction solution.

The content of DN^-, SO_4^{2-}, and NO_3^- in the permeate was detected by ion chromatography, and the purification effect of four NF membranes on ADN mixed acid reaction solution were evaluated. The ion chromatogram is shown in Fig. S3,† and the experimental results are shown in Fig. 10. As shown in Fig. 10, the retention rates DN^-, SO_4^{2-} and NO_3^- by the 200D NF were 57.83%, 98.51%, and 76.77%, respectively. The retention rates of DN^-, SO_4^{2-}, and NO_3^- by the 400D NF were 39.11%, 96.44%, and 52.89%, respectively. The retention rates of DN^-, SO_4^{2-}, and NO_3^- by the 600D NF were 20.67%, 96.57%, and 35.02%, respectively. The retention rates of DN^-, SO_4^{2-} and NO_3^- by the 800D NF were 21.08%, 96.65%, and 33.57%, respectively. All four NFs had good retention of SO_4^{2-} with retention rates above 96%, and the retention rates of NO_3^- were higher than those of DN^-, which provided the possibility of further optimization to improve the separation efficiency and yield. 600D NF was selected for further study, taking into account the retention effect of four types of NFs on ADN, SO_4^{2-}, and NO_3^- and the yield of ADN.

3.3 Influence of operating parameters

NF separates salt ions and small molecules of different valence forms through pore size sieving, dielectric repulsion, electro-static interaction, and their corresponding combined mecha-nisms. This process is often influenced by the nature of the NF itself and the operating parameters, and the selection of suit-able operating parameters is important for obtaining efficient separation efficiency and cost control. In this study, the optimal filtration parameters were obtained by comparing the effects of pressure, temperature, and original solution concentration of 600D NF for ADN separation to achieve efficient separation and purification of ADN.

3.3.1 Effect of pressure. Pressure is an important param-eter in the membrane separation process, and different membrane elements usually need to match the regulated pressure parameters in order to achieve the desired filtration effect. Different operating pressures have significant effects on solute retention, and some researchers have demonstrated that the change in the retention of divalent salt ions by NFs differs by a factor of two when the pressure is reduced by a factor of two under certain conditions.[55] In this study, the effect of operating pressure on the retention of SO_4^{2-}, and, and NO_3^- in the

Fig. 9 Decolorization effect of 200D, 400D, 600D, and 800D NFs on the raw synthetic solution. Number 1 is the raw synthetic solution, numbers 2, 4, 6, and 8 are the concentrated solutions of 200D, 400D, 600D, and 800DNFs, numbers 3, 5, 7, and 9 are the permeate solutions of 200D,400D, 600D, and 800D NFs

© 2023 The Author(s). Published by the Royal Society of Chemistry

original solution by 600D NF was investigated, and the results are shown in Fig. 11. It can be seen from Fig. 11 that the retention of SO_4^{2-} and ADN by 600D NF does not change much and the retention of NO_3^- increases significantly when the operating pressure increases. Ali et al.[56] found a similar phenomenon in the filtration of synthetic NO_3^- solutions using GE's DK and DL-type NFs. Therefore, in order to obtain a purer ADN solution during the filtration of the crude ADN solution, the operating pressure should be increased appropriately to increase the retention of NO_3^-, based on this, 2 MPa was used as the standard pressure in the subsequent experiments of this study to investigate other influencing factors.

3.3.2 Effect of temperature. Temperature is an important parameter affecting the membrane filtration process, which mainly affects the membrane filtration effect by influencing the nature of the filtration solution and the surface properties of the membrane. The temperature of the original filtration solution was controlled by a low-temperature thermostat to investigate the effect of different temperatures on the filtration effect. From Fig. 12, it can be seen that the effect of temperature change on the retention of solutes in 600D NFs is relatively small. When the temperature increases, the SO_4^{2-} retention takes the lead in increasing and then decreases, which is mainly because the

permeate flux decreases due to the contraction of membrane pores at low temperatures, thus affecting the dielectric repulsion effect at the solute–membrane interface leading to the decrease of retention rate. In addition, the solubility of solutes increases when the temperature rises, leading to a decrease in the retention rate, and eventually, the high temperature hinders the filtration effect of the experiment. Similar experimental results were obtained by Ismail[57] in the filtration of ammonium nitrate using TFC-S NFs, where the effect of temperature on the retention of NF solutes was mainly caused by changes in the fluidic properties of the solvent and the response of the membrane surface to temperature.

3.3.3 Influence of the concentration of the original solution. The concentration of solute is an important factor affecting the interception effect, which mainly affects the desalination effect of NF by affecting the transmembrane osmotic pressure. In the industrial membrane separation process, the concentration of the solute is a parameter that needs to be accurately controlled. In this study, the effect of the raw synthetic solution concentration on filtration was investigated by diluting the prepared ADN raw synthetic solution with ultrapure water. As shown in Fig. 13, the retention rate of solutes by NFs increased with the increase of solution dilution, in which the retention effect of SO_4^{2-} and NO_3^- increased significantly, this is mainly because in the process of solute
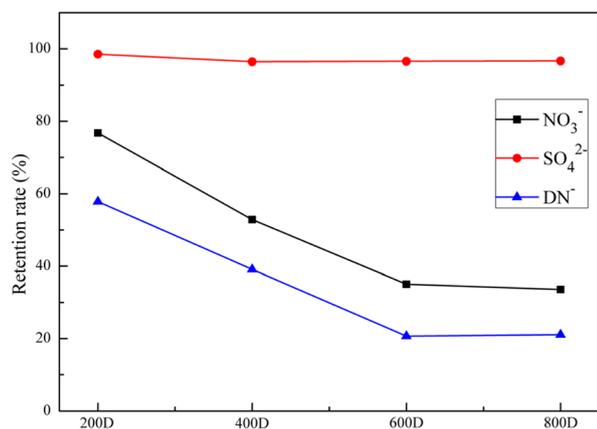

Fig. 10 Retention effect of 200D, 400D, 600D and 800D NFs on DN^-, SO_4^{2-} and NO_3^-. Test conditions: 0.5 MPa, 25 °C, undiluted.
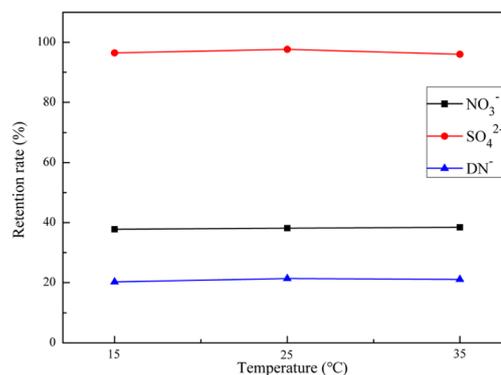

Fig. 12 Effect of temperature variation on the retention of different solutes by 600D NF. Test conditions: 2 MPa, undiluted.
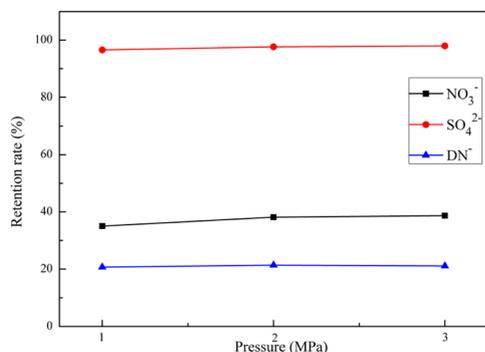

Fig. 11 Effect of pressure variation on the retention of different solutes by 600D NF. Test conditions: 25 °C, undiluted.
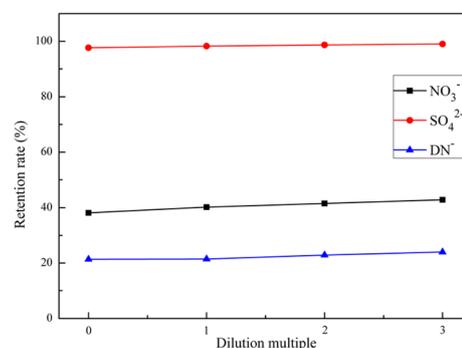

Fig. 13 Effect of dilution on the retention of different solutes by 600D NF. Test conditions: 2 MPa, 25 °C.
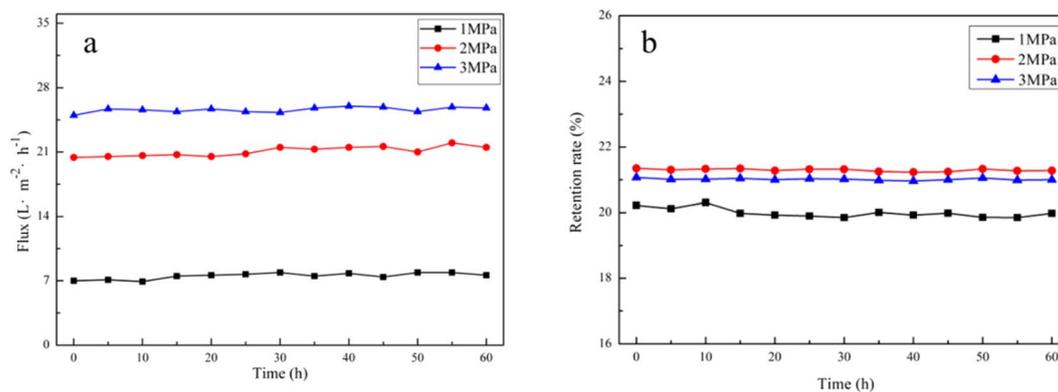
Fig. 14 Variation of membrane permeability of ADN raw synthetic solution filtered by 600D NF: (a) flux, (b) retention rate. Test conditions: 25 °C, 1× dilution.

separation by NF, as a large amount of solvent passes through the membrane into the permeate, the volume of retained liquid is concentrated, thus the concentration of solute increases, and the polarization effect of the concentration difference between the two sides of the membrane is significant, resulting in higher osmotic pressure and lower retention rate.[58,59] The higher the concentration of raw material liquid, the more obvious this effect is, so when the higher the dilution, the less obvious the decrease of retention rate brought by the concentration polarization effect, and thus the higher the retention rate. Considering the need of purified ADN solution to concentrate crystallization and the influence of the filtration rate, 1× dilution of ADN raw synthetic solution is the optimal filtration condition.

3.4 Variation of membrane flux

Membrane permeability is a key parameter affecting the stable operation of the NF process. In this study, the membrane permeability variation curves of 600D NF separation of ADN raw synthetic solution were monitored by long-term experiments for 60 hours. As shown in Fig. 14(a), the flux of 600D NF was stabilized at about $7 \text{ L m}^{-2} \text{ h}^{-1}$, $20 \text{ L m}^{-2} \text{ h}^{-1}$, $25 \text{ L m}^{-2} \text{ h}^{-1}$ under 1.0 MPa, 2.0 MPa, and 3.0 MPa filter pressure, respectively. As shown in Fig. 14(b), the retention rate of 600D NF was around 21% at the basic temperature under 1.0 MPa, 2.0 MPa, and 3.0 MPa. This indicates that the purification of salt ions

from ADN raw synthetic solution using conventional NF has a large potential for industrial application, and provides theoretical support for the large-scale purification preparation of ADN.

3.5 Improved filtering method

In order to obtain higher purity ADN and fully recycled ADN in the raw synthetic solution, the filtration method was improved by multistage cycling, as shown in Fig. 15. The concentration of the latter stage is driven into the upper stage for filtration again. Based on similar concepts, we also proposed a new and potentially cost-effective preparation method for obtaining high-purity ADN. The process design principles proposed in this method can be flexibly adjusted according to specific treatment objectives. Our team has applied for a Chinese invention patent for this method. Another Chinese invention patent related to the preparation of high-purity ADN has been authorized by our team and its engineering application is in progress.[60] When the first level is concentrated to a certain volume, an appropriate amount of water is constantly added for dialysis until the recovery rate reaches more than 99%.

3.6 Characterization and purity analysis of ADN

The purified ADN was characterized by UV-visible, IR, and Raman spectroscopy techniques, and the purity of the purified ADN was analyzed by ion chromatography, as shown in Fig. 16.
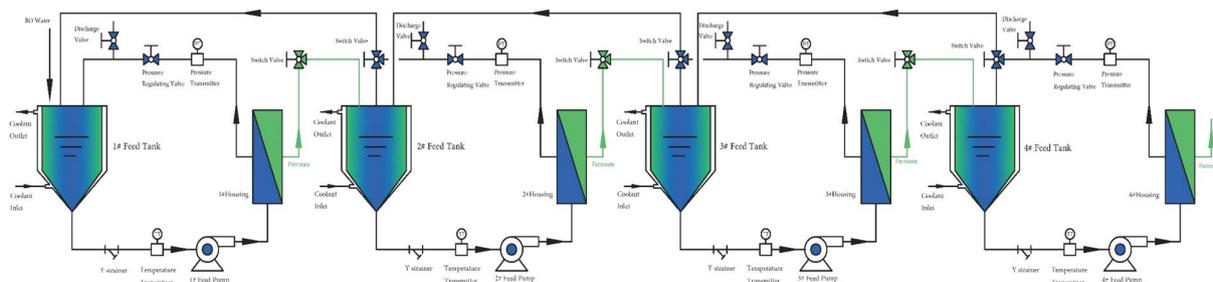

Fig. 15 Improved filtering method of raw synthetic solution.

© 2023 The Author(s). Published by the Royal Society of Chemistry

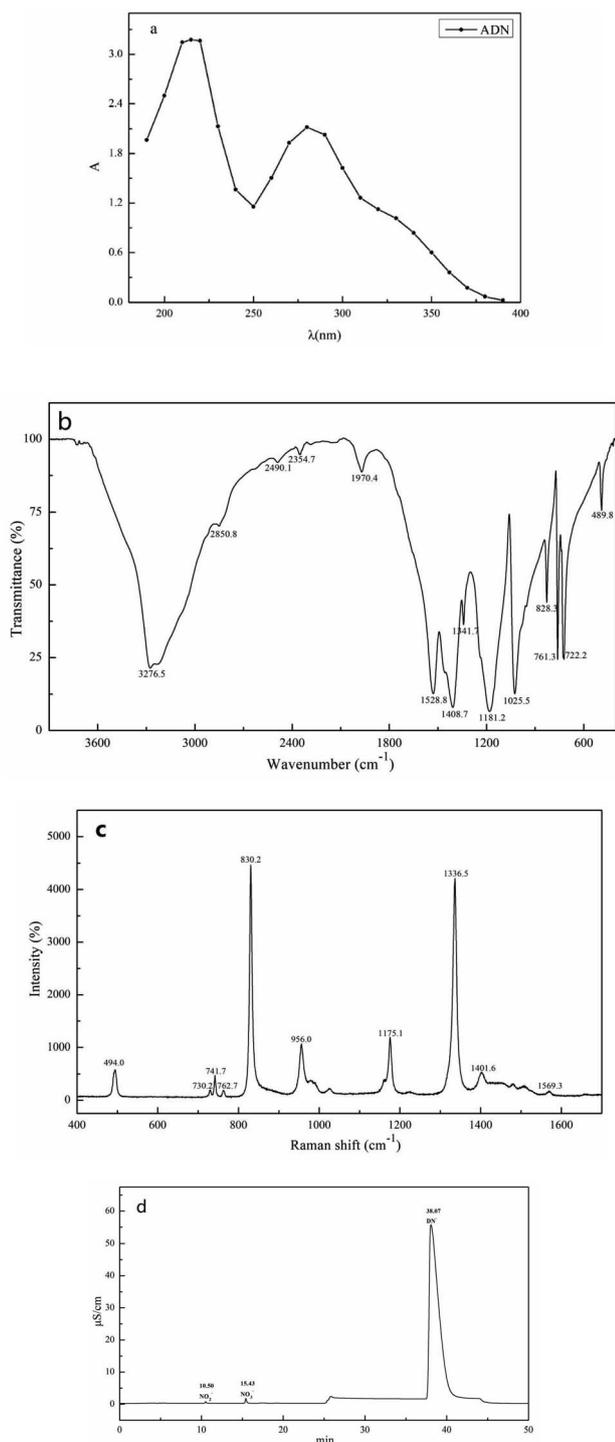| Sample (mg/L)	NO₂⁻	NO₃⁻	SO₄²⁻	DN⁻	Relative purity (%)
ADN	5.229	33.89	2.465	27638	99.849

Fig. 16   UV-visible spectrum (a), IR spectrum (b), Raman spectrum (c) and ion chromatogram (d) of the purified ADN.

Fig. 16(a) shows the UV visible spectrum of ADN. It can be seen from Fig. 16(a) that the ADN purified by 600D NF membrane has the maximum UV absorption peaks at 212 nm and 284 nm, which is consistent with the maximum UV absorption peaks of ADN reported in the literature.[61] Fig. 16(b) shows the infrared

spectrum of ADN. It can be seen from Fig. 16(b) that 1528 cm^{-1} and 1408 cm^{-1} are the absorption peaks of –NO$_2$ anti-symmetric stretching vibrations, 1341 cm^{-1} and 1181 cm^{-1} are the absorption peaks of the –NO$_2$ symmetric stretching vibration, 1025 cm^{-1} is the absorption peak of the N$_3$ antisymmetric stretching vibration, 828 cm^{-1} is the absorption peak of –NO$_2$ shear bending vibration, 761 cm^{-1} and 489 cm^{-1} are the absorption peaks of –NO$_2$ swing vibration, which are consistent with the ADN characteristic peaks reported in the reference.[61] Fig. 16(c) shows the Raman spectrum of ADN. It can be seen from Fig. 16(c) that 1569 cm^{-1} and 1401 cm^{-1} are the anti-symmetric stretching vibration absorption peaks of –NO$_2$, 1336 cm^{-1} and 1175 cm^{-1} –NO$_2$ are the symmetric stretching vibration absorption peaks, 956 cm^{-1} is the antisymmetric stretching vibration absorption peak of N$_3$, 830 cm^{-1} is the shear bending vibration absorption peak of –NO$_2$, and 494 cm^{-1} is the in-plane rocking vibration absorption peak, which is consistent with the ADN characteristic peak reported in reference. The successful synthesis of ADN was demonstrated through UV, infrared, and Raman spectroscopy characterization.

The purity of ADN purified by fourth-stage cyclic NF was analyzed through ion chromatography, as shown in Fig. 16(d). The content of NO$_2^-$, NO$_3^-$, and SO$_4^{2-}$ in the spectrum was all within 0.2%. The table shows the concentration of NO$_2^-$, NO$_3^-$, SO$_4^{2-}$, and DN$^-$ after the fourth stage cyclic NF, with an ADN purity of 99.8%, indicating that this method can obtain high-purity ADN while maintaining a high yield.

4.   Conclusion

In this study, ammonium sulfamate was used as raw material to prepare crude ADN by nitration. NF was prepared by interfacial polymerization, and then a membrane purification system was designed and prepared according to the characteristics of the ADN synthetic material system, and the process for rapid preparation of high-purity ADN was obtained. The separation and recovery of by-products and impurities (such as sulfate and nitrate) produced during the whole process of ADN preparation were investigated by NF technology. NF has the ability to separate the inorganic salt ions in the raw synthetic solution of ADN prepared by the nitrous-sulfur mixed acid method. Increasing the operating pressure had less effect on the retention of SO$_4^{2-}$ in the mixed system, but it could lower the retention of ADN, and the highest retention of SO$_4^{2-}$ was achieved at 25 °C. The dilution of the feed solution could improve the retention of solutes by the NF. In addition, the fluxes of the 600D NF were stable during filtration, which has the potential for engineering amplification.

As a new oxidant with excellent performance, high energy, and green characteristics, ADN is one of the typical representatives of new energetic materials. The mixed acid production process of ADN is also a classic production process of HEDM. This technology has the potential for the large-scale production of ADN and also provides a reference for the safe, efficient, and cheap preparation of HEDM. Our team has applied for a Chinese invention patent for the above technology, and

further process optimization, such as automation and continuous preparation process, is in progress.

Conflicts of interest

The authors declare that they have no known competing financial interests or personal relationships that could have appeared to influence the work reported in this paper.

Acknowledgements

References

1 Y. X. Tang, C. L. He, G. H. Imler, D. A. Parrish and J. M. Shreeve, Aminonitro Groups Surrounding a Fused Pyrazolotriazine Ring: A Superior Thermally Stable and Insensitive Energetic Material, *ACS Appl. Energy Mater.*, 2019, **2**(3), 2263–2267.

2 T. Yan, C. Yang, J. Ma, G. Cheng and H. Yang, Intramolecular integration of multiple heterocyclic skeletons for energetic materials with enhanced energy & safety, *Chem. Eng. J.*, 2022, **428**, 131400.

3 T. Brinck, *Green energetic materials*, John Wiley & Sons Ltd, 2014.

4 Y. C. Li, C. Qi, S. H. Li, H. J. Zhang, C. H. Sun, Y. Z. Yu and S. P. Pang, 1, 1′-Azobis-1, 2, 3-triazole: a high-nitrogen compound with stable N8 structure and photochromism, *J. Am. Chem. Soc.*, 2010, **132**, 12172–12173, DOI: 10.1021/ja103525v.

5 V. Thottempudi, F. Forohor, D. A. Parrish and J. M. Shreeve, Tris (triazolo) benzene and its derivatives: high-density energetic materials, *Angew. Chem.*, 2012, **51**, 9881–9885, DOI: 10.1002/ange.201205134.

6 S. H. Li, Y. Wang, C. Qi, X. X. Zhao, J. C. Zhang, S. W. Zhang and S. P. Pang, 3D energetic metal–organic frameworks: synthesis and properties of high energy materials, *Angew. Chem., Int. Ed.*, 2013, **52**, 14031–14035, DOI: 10.1002/anie.201307118.

7 Y. X. Tang, H. W. Yang, B. Wu, X. H. Ju, C. X. Lu and G. Cheng, Synthesis and characterization of a stable, catenated N11 energetic salt, *Angew. Chem., Int. Ed.*, 2013, **52**, 4975–4977, DOI: 10.1002/anie.201300117.

8 Q. Sun, N. Ding, C. F. Zhao, J. Ji, S. H. Sheng and S. P. Pang, Positional isomerism for strengthening intermolecular interactions: toward monocyclic nitramino oxadiazoles with enhanced densities and energies, *Chem. Eng. J.*, 2022, **427**, 130912, DOI: 10.1016/j.cej.2021.130912.

9 V. S. Sergey, A. L. Antonina, T. C. Yuliya and V. S. Gennady, Methods of synthesis and properties of hexanitrohexaazaisowurtzitane, *Russ. Chem. Rev.*, 2005, **74**(8), 757, DOI: 10.1070/RC2005v074n08ABEH001179.

10 X.-X. Zhang, Z.-J. Yang, F. Nie and Q.-L. Yan, Recent advances on the crystallization engineering of energetic materials, *Energ. Mater. Front.*, 2020, **1**(3), 141–156, DOI: 10.1016/j.enmf.2020.12.004.

11 Y. Wang, D. Han, X. Zhou, Z. Zhang, J. Gong, H. Li and Q. Zhang, The preparation of higher performance solid form of DATNBI based on rapid *in situ* solvate-mediated phase transition mechanism, *Chem. Eng. J.*, 2023, **456**, 141052, DOI: 10.1016/j.cej.2022.141052.

12 L. Li, H. Ling, J. Tao, C. Pei and X. Duan, Microchannel-confined crystallization: shape-controlled continuous preparation of a high-quality CL-20/HMX cocrystal, *CrystEngComm*, 2022, **24**(8), 1523–1528, DOI: 10.1039/d1ce01524a.

13 S. Zhang, L.-w. Zhan, G.-k. Zhu, Y.-y. Teng, X.-g. Wu, J. Hou and B.-d. Li, Continuous, safe and large-scale preparation of insensitive high-energy TATB/HMX composite particles by microfluidic self-assembly technology, *Chem. Eng. Sci.*, 2022, **264**, 118160, DOI: 10.1016/j.ces.2022.118160.

14 F. Pessina, F. Schnell and D. Spitzer, Tunable continuous production of RDX from microns to nanoscale using polymeric additives, *Chem. Eng. J.*, 2016, **291**, 12–19, DOI: 10.1016/j.cej.2016.01.083.

15 S. Li, Y. Wang, C. Qi, X. Zhao, J. Zhang, S. Zhang and S. Pang, 3D Energetic Metal–Organic Frameworks: Synthesis and Properties of High Energy Materials, *Angew. Chem., Int. Ed.*, 2013, **52**(52), 14031–14035, DOI: 10.1002/anie.201307118.

16 E. L. Dreizin and M. Schoenitz, Mechanochemically prepared reactive and energetic materials: a review, *J. Mater. Sci.*, 2017, **52**(20), 11789–11809, DOI: 10.1007/s10853-017-0912-1.

17 F. P. Fabbiani and C. R. Pulham, High-pressure studies of pharmaceutical compounds and energetic materials, *Chem. Soc. Rev.*, 2006, **35**(10), 932–942, DOI: 10.1039/b517780b.

18 S.-N. Luo and M. Gozin, Energetic Materials: Novel Syntheses and Diagnostics, *Engineering*, 2020, **6**(9), 974–975, DOI: 10.1016/j.eng.2020.07.002.

19 T. J. Fleck, A. K. Murray, I. E. Gunduz, S. F. Son, G. T. C. Chiu and J. F. Rhoads, Additive manufacturing of multifunctional reactive materials, *Addit. Manuf.*, 2017, **17**, 176–182, DOI: 10.1016/j.addma.2017.08.008.

20 T. Wang, X. Zhou, S. L. Hao, S. H. Zhang, R. J. Gou and H. Z. Li, Green Crystallization of HMX Based on Membrane Separation: Preparation and Characterization, *Chin. J. Energ. Mater.*, 2023, **31**(1), 8–17.

21 D. Trache, F. Maggi, I. Palmucci and L. T. DeLuca, Thermal behavior and decomposition kinetics of composite solid propellants in the presence of amide burning rate suppressants, *J. Therm. Anal. Calorim.*, 2018, **132**(3), 1601–1615.

22 D. Zhai, C. Ma, P. Ma, Y. Pan, L. Hao, X. Liu and J. Jiang, Theoretical insight into different energetic groups on the performance of energetic materials featuring RDX ring, *Fuel*, 2021, **294**, 120497.

23 J. Jos and S. Mathew, Ammonium nitrate as an eco-friendly oxidizer for composite solid propellants: promises and

challenges, *Crit. Rev. Solid State Mater. Sci.*, 2017, **42**(6), 470–498.

24 Y. Wang, S. Song, C. Huang, X. Qi, K. Wang, Y. Liu and Q. Zhang, Hunting for advanced high-energy-density materials with well-balanced energy and safety through an energetic host–guest inclusion strategy, *J. Mater. Chem. A*, 2019, **7**(33), 19248–19257.

25 C. Griego, N. Yilmaz and A. Atmanli, Analysis of aluminum particle combustion in a downward burning solid rocket propellant, *Fuel*, 2019, **237**, 405–412.

26 A. Mezroua, K. Khimeche, M. H. Lefebvre, M. Benziane and D. Trache, The influence of porosity of ammonium perchlorate (AP) on the thermomechanical and thermal properties of the AP/polyvinylchloride (PVC) composite propellants, *J. Therm. Anal. Calorim.*, 2014, **116**(1), 279–286.

27 M. Kohga and S. Togo, Influence of iron oxide on thermal decomposition behavior and burning characteristics of ammonium nitrate/ammonium perchlorate-based composite propellants, *Combust. Flame*, 2018, **192**, 10–24.

28 M. C. Rehwoldt, Y. Yang, H. Wang, S. Holdren and M. R. Zachariah, Ignition of nanoscale titanium/potassium perchlorate pyrotechnic powder: reaction mechanism study, *J. Phys. Chem. C*, 2018, **122**(20), 10792–10800.

29 J. Y. Lyu, J. H. Yu, D. Y. Tang, W. He, B. W. Tao, X. Guo and Q. L. Yan, Unexpected burning rate independence of composite propellants on the pressure by fine interfacial control of fuel/oxidizer, *Chem. Eng. J.*, 2020, **388**, 124320.

30 P. Kumar, An overview on properties, thermal decomposition, and combustion behavior of ADN and ADN based solid propellants, *Def. Technol.*, 2018, **14**(6), 661–673.

31 X. Zhao, S. Li, Y. Wang, Y. Li, F. Zhao and S. Pang, Design and synthesis of energetic materials towards high density and positive oxygen balance by N-dinitromethyl functionalization of nitroazoles, *J. Mater. Chem. A*, 2016, **4**(15), 5495–5504.

32 H. M. Li, G. X. Li and L. Li, Comparative investigation on combustion characteristics of ADN-based liquid propellants in inert gas and oxidizing gas atmospheres with resistive ignition method, *Fuel*, 2023, **334**, 126742.

33 T. T. Vo, D. A. Parrish and J. M. Shreeve, Tetranitroacetimidic acid: a high oxygen oxidizer and potential replacement for ammonium perchlorate, *J. Am. Chem. Soc.*, 2014, **136**(34), 11934–11937.

34 H. Matsunaga, H. Habu and A. Miyake, Thermal behavior of new oxidizer ammonium dinitramide, *J. Therm. Anal. Calorim.*, 2013, **111**(2), 1183–1188.

35 H. Chen, L. Fu, R. Zhang, C. Lin, T. Jiang, X. Li and G. Li, Local energy market clearing of integrated ADN and district heating network coordinated with transmission system, *Int. J. Electr. Power Energy Syst.*, 2021, **125**, 106522.

36 J. Li, R. Yang, T. Zeng, J. Hu, W. Tang, Z. Liu and L. Gong, Preparation and growth mechanism of micro spherical ammonium dinitramide crystal based on ultrasound-assisted solvent-antisolvent method, *Ultrason. Sonochem.*, 2021, **78**, 105716.

37 M. Negri, M. Wilhelm, C. Hendrich, N. Wingborg, L. Gediminas, L. Adelöw, C. Maleix, P. Chabernaud, R. Brahmi and R. Beauchet, New technologies for ammonium dinitramide based monopropellant thrusters–The project RHEFORM, *Acta Astronaut.*, 2018, **143**, 105–117.

38 D. M. Badgujar, N. R. Bulakh, R. M. Wagh and M. B. Talawar, Synthesis, characterization and purity determination of ammonium dinitramide (ADN) and its precursors, *Sci. Technol. Energ. Mater.*, 2016, **77**, 59–64.

39 H. G. Jang, M. J. Sul, J. S. Shim, Y. C. Park and S. J. Cho, Scalable synthesis of high purities ammonium dinitramide and its decomposition characteristics, *J. Ind. Eng. Chem.*, 2018, **63**, 237–244.

40 A. Rahman, J. Chin and K. H. Cheah, Prilling and coating of ammonium dinitramide (ADN) solid green propellant in toluene mixture using ultrasound sonication, *Aerospace*, 2018, **5**(1), 29.

41 Y. Sugie and A. Miyake, Effect of the density of nitric acid on thermal behavior during sulfamate nitration, *J. Therm. Anal. Calorim.*, 2015, **121**(1), 275–279.

42 P. Kudryavtsev, Production technology development and creation of production of additives used in solid rocket propellants, *Sci. Isr.–Technol. Advantages*, 2014, **16**(3), 25–37.

43 H. Matsunaga, S. Yoshino, M. Kumasaki, H. Habu and A. Miyake, Aging characteristics of the energetic oxidizer ammonium dinitramide, *Sci. Technol. Energ. Mater.*, 2011, **72**(5–6), 131–135.

44 F. Y. Chen, C. L. Xuan, Q. Q. Lu, L. Xiao, J. Q. Yang, Y. B. Hu, G. P. Zhang, Y. L. Wang, F. Q. Zhao and G. Z. Hao, A review on the high energy oxidizer ammonium dinitramide: its synthesis, thermal decomposition, hygroscopicity, and application in energetic materials, *Def. Technol.*, 2023, **19**, 163–195, DOI: 10.1016/j.dt.2022.04.006.

45 W. Kim, Y. Kwon, S. Y. Hwang and Y. Jo, Comparative evaluation of purity of green energetic material (ammonium dinitramide) depending on refining method, *Korean J. Chem. Eng.*, 2017, **34**(6), 1693–1698.

46 Y. F. Pan, W. X. Liu and X. Zhao, Separation and purification of ADN by activated carbon adsorption, *Chin. J. Explos. Propellants*, 2017, **40**(4), 61–65.

47 M. Comet, C. Schwartz, F. Schnell, F. Oudot, B. Lallemand and D. Spitzer, New Detonating Compositions from Ammonium Dinitramide, *Propellants, Explos., Pyrotech.*, 2021, **46**(5), 742–750.

48 X. Feng, D. Peng, J. Zhu, Y. Wang and Y. Zhang, Recent advances of loose nanofiltrations for dye/salt separation, *Sep. Purif. Technol.*, 2022, **285**, 120228.

49 Y. Wang, S. Zhao, Z. Zha, Z. Wang and J. Wang, Host-guest nanofiltration membranes having amino-complexed cucurbituril supramolecular channel for monovalent/divalent salts separation, *Desalination*, 2022, **527**, 115582.

50 N. Hilal, H. Al-Zoubi, N. Darwish, A. Mohamma and M. A. Arabi, A comprehensive review of nanofiltration membranes: Treatment, pretreatment, modelling, and atomic force microscopy, *Desalination*, 2004, **170**(3), 281–308.

51 N. S. Suhalim, N. Kasim, E. Mahmoudi, I. J. Shamsudin, A. W. Mohammad, F. Mohamed Zuki and N. L. A. Jamari, Rejection Mechanism of Ionic Solute Removal by

nanofiltration membranes: An Overview, *Nanomaterials*, 2022, **12**(3), 437.

52 L. Yao, Z. Qin, Q. Chen, M. Zhao, H. Zhao, W. Ahmad, L. Fan and L. Zhao, Insights into the nanofiltration separation mechanism of monosaccharides by molecular dynamics simulation, *Sep. Purif. Technol.*, 2018, **205**, 48–57.

53 Y. Zhao, T. Tong, X. Wang, S. Lin, E. M. Reid and Y. Chen, Differentiating solutes with precise nanofiltration for next generation environmental separations: a review, *Environ. Sci. Technol.*, 2021, **55**(3), 1359–1376.

54 R. Raghavan and S. Jacob, Ion Chromatographic Analysis of Ammonium Dinitramide–Oxidizer for Propellant and Pyrotechnic Applications, *Propellants, Explos., Pyrotech.*, 2013, **38**(2), 273–277.

55 B. Yuan, P. Li, H. Sun, S. Zhao, P. Li, H. Sun and Q. J. Niu, Novel non-trimesoyl chloride based polyamide membrane with significantly reduced Ca^{2+} surface deposition density, *J. Membr. Sci.*, 2019, **578**, 251–262.

56 R. D. Ali and U. Tarık, Impact of operating parameters on the nitrate removal by nanofiltration, *Adv. in Ecological and Environ. Res.*, 2018, **3**(3), 41–57.

57 K. Ismail, Effect of operating conditions on the separation of ammonium and nitrate ions with nanofiltration and reverse osmosis membranes, *J. Environ. Sci. Health, Part A*, 2002, **37**(7), 1347–1359.

58 X. Li, S. Tan, J. Luo and M. Pinelo, Nanofiltration for separation and purification of saccharides from biomass, *Front. Chem. Sci. Eng.*, 2021, **15**(4), 837–853.

59 M. Peydayesh, T. Mohammadi and S. K. Nikouzad, A positively charged composite loose nanofiltration membrane for water purification from heavy metals, *J. Membr. Sci.*, 2020, **611**, 118205.

60 Y. C. Li, H. Y. Zhu, H. Y. Sun, Y. H. Liu, X. Y. Miao, P. X. Zhang, F. Cui and Q. H. Qin, A method for separation and preparation of high energy oxidant ammonium dinitramide, CN113336241A, 2022.

61 W. Kim, Y. Kwon, S. Y. Hwang and Y. Jo, Comparative evaluation of purity of green energetic material (ammonium dinitramide) depending on refining method, *Korean J. Chem. Eng.*, 2017, **34**(6), 1693–1698.